2005 American Control Conference
June 8-10, 2005. Portland, OR, USA



# Predictive Control of Particle Size Distribution in Protein Crystallization

Dan Shi, Prashant Mhaskar, Nael H. El-Farra and Panagiotis D. Christofides*
Department of Chemical Engineering, University of California, Los Angeles, CA 90095-1592

*Abstract*— **This work focuses on control of a batch protein crystallization process that produces tetragonal hen egg-white (HEW) lysozyme crystals. First, a population balance model, which incorporates experimentally-determined nucleation and growth rates, is used to simulate the evolution of the entire crystal size distribution (CSD). Then, a reduced-order model, which describes the evolution of the dominant moments of the CSD and of the solute concentration and crystallizer temperature, is derived and used for controller design. A predictive controller is designed to achieve the objective of maximizing the volume-averaged crystal size while respecting constraints on the manipulated input variable and the process state variables including constraints on the shape of the CSD. Simulation results demonstrate that the proposed predictive controller is able to increase the volume-averaged crystal size by 30% and 8.5% compared to Constant Temperature Control (CTC) and Constant Supersaturation Control (CSC) strategies, respectively, while reducing the number of fine crystals produced. The robustness of the proposed control method with respect to: (a) plant-model mismatch, and (b) open-loop operation, is also successfully demonstrated.**

## I. Introduction

Proteins play a vital role in all biological processes. In addition to constructing large-scale biological structures, such as muscle fibers, smaller protein molecules can function as antibodies, which help the immune system to destroy invading substances like viruses and bacteria, and enzymes, which can catalyze the synthesis of complex compounds, transformation of complex substances into simple ones, or the generation of energy in organisms. The structure of a protein molecule determines its specific biological function. Many pharmaceuticals act by binding to and blocking an active site of a protein. To grow required protein crystals, which are necessary to study the structure of proteins with molecular weight over 20,000, extensive efforts have been focused on the study of nucleation and growth mechanisms under various operating conditions. These efforts not only benefit the determination of the protein structure, but also provide, through an understanding of the nucleation and growth mechanisms, a way of determining the operating conditions necessary to achieve protein crystals of desired properties (often expressed in the form of a desired crystal size distribution (CSD)). In the pharmaceutical industry, the size distribution of the protein crystal is a very critical variable and in many applications a predetermined, typically narrow, CSD is necessary in order to guarantee a desired drug delivery performance.

*Corresponding author: Panagiotis D. Christofides (pdc@seas.ucla.edu)

Protein crystals intrinsically grow much slower than most inorganic crystals at the same supersaturation [1]. This is probably one of the reasons why it has been widely believed that implementation of advanced control algorithms is not important for growing perfect crystals in protein crystallization. However, experimental results show that even in protein crystallization processes, certain growth conditions lead to crystal defect formation (for example, the structural defect density increases when the growth rate is relatively high [2]), which necessitates appropriately choosing the operating conditions. Furthermore, for a given choice of operating conditions, it is critical to implement real-time control to mitigate the affect of disturbances that might drive the operating conditions off the desired values. While numerous experimental studies of the nucleation and growth mechanisms of protein crystallization have been carried out, very few results on control of protein crystallization are available ([3], [4]).

The mathematical models of particulate processes, including crystallization, are typically obtained through the application of population, material and energy balances and consist of systems of nonlinear partial integro-differential equations that describe the evolution of the particle size distribution, coupled with systems of nonlinear ordinary differential equations (ODEs) that describe the evolution of the state variables of the continuous phase. There is an extensive literature on population balance modeling, numerical solution, and dynamical analysis of particulate processes, see, for example, [5], [6], [7], [8], [9], [10], [11], [12]; see also [13] for further details and references. Early work on control of particulate processes focused mainly on the understanding of fundamental control-theoretic properties of population balance models (PBMs), e.g., [14], and the application of conventional control schemes to crystallizers and emulsion polymerization processes, e.g., [15], [16], [17], [26] and the references therein. More recently, the realization that PBMs – owing to their infinite-dimensional nature – cannot be used directly for the synthesis of practically implementable controllers, has motivated significant research work on the development of a general order reduction procedure, based on combination of the method of weighted residuals and approximate inertial manifolds, which allows deriving low-order ODE approximations that capture the dominant dynamics of particulate processes and can, therefore, serve as an appropriate basis for the design of low-order controllers that can be readily implemented in practice, see, for example, [18]. This approach subsequently

0-7803-9098-9/05/$25.00 ©2005 AACC

laid the foundation for the development of a systematic framework for solving a number of important control problems for particulate processes, including the problem of dealing with highly nonlinear behavior (e.g., owing to complex growth, nucleation, agglomeration and breakage mechanisms, and the Arrhenius dependence of nucleation laws on solute concentration in crystallizers [18]), the problem of model uncertainty [19], and the problem of control under actuator constraints [20].

In the operation of particulate processes, constraints typically arise due to physical limitations on the capacity of control actuators and/or desired restrictions on the process state variables, such as temperature and the particle size distribution (e.g., crystal concentration and total particle size), in order to meet some safety or product quality requirements. In current industrial practice, the achievement of optimal performance, subject to input and state constraints, relies to a large extent on the use of predictive control policies which are well known for their ability to handle multi-variable interactions, constraints, and optimization requirements, all in a consistent, systematic manner [21]. Unlike open-loop model-based optimal control policies (where the optimal operating conditions are calculated off-line), in predictive control, the control action is computed by solving repeatedly, on–line, a constrained optimization problem at each sampling time. Owing to this, predictive control has the ability to suppress the influence of external disturbances and tolerate model inaccuracies (because of the use of feedback) and force the system to follow an optimal trajectory that respects constraints on the operating conditions.

In this work, we focuse on control of a batch protein crystallization process that produces tetragonal hen egg-white (HEW) lysozyme crystals. First, a population balance model, which incorporates experimentally-determined nucleation and growth rates, is used to simulate the evolution of the entire crystal size distribution (CSD). Then, a reduced-order model, which describes the evolution of the dominant moments of the CSD and of the solute concentration and crystallizer temperature, is derived and used for controller design. A predictive controller is designed to achieve the objective of maximizing the volume-averaged crystal size while respecting constraints on the manipulated input variable and the process state variables including constraints on the shape of the CSD. Simulation results demonstrate that the proposed predictive controller is able to increase the volume-averaged crystal size by 30% and 8.5% compared to Constant Temperature Control (CTC) and Constant Supersaturation Control (CSC) strategies, respectively, while reducing the number of fine crystals produced. The robustness of the proposed control method with respect to: (a) plant-model mismatch, and (b) open-loop operation, is successfully demonstrated.

## II. Modeling of a batch process for protein crystallization

In this work, we consider a batch crystallizer used to produce the tetragonal HEW lysozyme crystals from supersaturated solution. The population balance model of this crystallizer describes the evolution of the crystal size distribution, $n(r,t)$, under the joint effects of nucleation ($B$) and crystal growth ($G$). The evolution of the solute concentration, $C$, and crystallizer temperature, $T$, are described by two ODEs. The process model has the following form:

$$\begin{aligned} &\frac{\partial n(r,t)}{\partial t} + G(t)\frac{\partial n(r,t)}{\partial r} = 0, \quad n(0,t) = \frac{B(t)}{G(t)} \\ &\frac{dC}{dt} = -24\rho k_v G(t)\mu_2(t) \\ &\frac{dT}{dt} = -\frac{UA}{MC_p}(T - T_j) \end{aligned} \tag{1}$$

where $\rho$ is the density of the crystals, $k_v$ is the volumetric shape factor, $U$ is the overall heat-transfer coefficient, $A$ is the total heat-transfer surface area, $M$ is the mass of solvent in the crystallizer, $C_p$ is the heat capacity of the solution and $\mu_2 = \int_0^\infty r^2 n(r,t)dr$ is the second moment of the CSD. Note that because of the tetragonal form of the crystals and the existence of about 46% of solution in each crystal [22], the volumetric shape factor, $k_v$, is set to 0.54. The nucleation rate, $B(t)$, and the growth rate, $G(t)$, are given by [23]:

$$\begin{aligned} B(t) &= k_a C exp\left(-\frac{k_b}{\sigma^2}\right) \\ G(t) &= k_g \sigma^g \end{aligned} \tag{2}$$

where $\sigma$, the supersaturation, is a dimensionless variable defined as $\sigma = ln(C/C_s)$, $C$ is the solute concentration, and $C_s$ is the saturation concentration of the solute, and is calculated by Eq.3 below. $g$ is the exponent relating growth rate to the supersaturation. The parameters values are obtained by analyzing experimental results (details can be found in [23]), and are reported in Table I.

$$\begin{aligned} C_s(T) = \; & 1.0036 \times 10^{-3} T^3 + 1.4059 \times 10^{-2} T^2 \\ & -0.12835T + 3.4613 \end{aligned} \tag{3}$$

TABLE I

Parameter values for the batch crystallizer of Eqs.1–2.

| | | | |
|---|---|---|---|
| $k_a$ | $1044.4/(min\ cm^3)$ | $k_g$ | $3.1451 \times 10^{-9} cm/min$ |
| $k_b$ | 51.33 | $g$ | 5.169 |
| $k_v$ | 0.54 | $\rho$ | $1.40 \times 10^3 mg/cm^3$ |
| $U$ | $1800 kJ/m^2 \cdot hr \cdot K$ | $A$ | $0.25 m^2$ |
| $M$ | $10 kg$ | $C_p$ | $4.13 kJ/K \cdot kg$ |

Owning to the fact that the dominant dynamics of the crystallizer are characterized by a small number of degrees of freedom, the method of moments [24] (see also [13], [25]) is applied to the system of Eq.1 to derive an approximate ODE model. Defining the $i$th moment of $n(r,t)$ as:

$$\mu_i = \int_0^\infty r^i n(r,t)dr, \quad i = 0, \ldots, \tag{4}$$

multiplying the population balance in Eq.1 by $r^i$, and integrating over all crystal sizes, the following infinite set of ordinary differential equations, which describes the rate of change of the moments of the crystal size distribution, solute concentration and temperature, is obtained:

$$\begin{aligned} \frac{d\mu_0}{dt} &= B(t) \\ \frac{d\mu_i}{dt} &= iG(t)\mu_{i-1}(t), \quad i = 1, 2, ... \\ \frac{dC}{dt} &= -24\rho k_v G(t)\mu_2(t) \\ \frac{dT}{dt} &= -\frac{UA}{MC_p}(T - T_j) \end{aligned} \tag{5}$$

Since the control objective will be to maximize the volume-averaged crystal size, defined as $\mu_4/\mu_3$ (see section III below), following truncation of the system of Eq.5 will be used on the basis for controller design.

$$\begin{aligned} \frac{d\mu_0}{dt} &= B(t) \\ \frac{d\mu_i}{dt} &= iG(t)\mu_{i-1}(t), \quad i = 1, ..., 4 \\ \frac{dC}{dt} &= -24\rho k_v G(t)\mu_2(t) \\ \frac{dT}{dt} &= -\frac{UA}{MC_p}(T - T_j) \end{aligned} \tag{6}$$

## III. Predictive control of the batch protein crystallizer

The most important objective of the control of the batch protein crystallizer is to achieve a desired particle size distribution at the end of the batch and to satisfy state and control constraints during the whole batch run. Significant previous work has focused on CSD control in batch crystallizers. In [28], an open-loop optimal control strategy was derived, where the objective function involves maximization of the crystal size and the cooling curve is the decision variable. In [21], a method was developed for assessing parameter uncertainty and studied its effects on the open-loop optimal control strategy, which maximized the weight mean size of the product. To improve the product quality expressed in terms of the mean size and the width of the distribution, an on-line optimal control methodology was developed for a seeded batch cooling crystallizer [27], [29]. The crystals studied in these works are mostly inorganic (e.g., potassium sulphate), and their crystallization behavior is significantly different from those of proteins, due to the higher molecular weight and more complex structure of the protein molecules. In these previous works, most efforts were focused on the open-loop optimal control of the batch crystallizer, i.e., the optimal operating condition was calculated off-line. The successful application of such a control strategy relies, to a large extent, on the accuracy of the models. Furthermore, an open-loop control strategy may not be able to guide the system to follow the optimal trajectory because of the ubiquitous existence of modeling error and the effect of disturbances.

In this work, we focus on developing a predictive control system to maximize the volume-averaged tetragonal lysozyme crystal size (i.e., $\mu_4/\mu_3$), by manipulating the jacket temperature, $T_j$. The principal moments are calculated from the on-line measurements of CSD, $n$, which can be obtained by measurement techniques such as the laser light scattering method. The solute concentration and crystallizer temperature are also assumed to be measured in real time. In the closed-loop control structure, the PBM, together with the mass and energy balances of Eq.1, are used to describe the process while the reduced-order model of Eq.6 is used within the predictive controller for the purpose of prediction. The PBM is utilized to simulate the value of the state variables ($n$, $C$, $T$) at $t_i = i\Delta t$, where $i$=1,2,...,$m$, $m = t_f/\Delta t$, and $t_f$ is the length of the crystallization period. The values of the moments ($\mu_j(t_i)$, $j$=0,...,4) are calculated from the CSD at every $t_i$, $n(r, t_i)$. The values of $\mu_j(t_i)$, $C(t_i)$, $T(t_i)$, and the optimal trajectory of $T_j$ solved at the previous time step, are used as the initial values for the reduced-order model in the predictive controller to solve an optimization problem over a horizon length of $t_f - t_i$. The first step of the solution ($T_j$) is implemented to generate the value of the state variables at the end of the next time step, $t_{i+1}$. This procedure is repeated every $\Delta t$ until the end of the batch run.

Manipulated input limitations, as well as specifications on supersaturation and crystallizer temperature are incorporated as input and state constraints on the optimization problem, which takes the form:

$$\begin{aligned} \min \quad & -\frac{\mu_4(t_f)}{\mu_3(t_f)} \\ s.t. \quad & \frac{d\mu_0}{dt} = k_a Cexp\left(-\frac{k_b}{\sigma^2}\right) \\ & \frac{d\mu_i}{dt} = ik_g\sigma^g\mu_{i-1}(t), \quad i = 1, ..., 4 \\ & \frac{dC}{dt} = -24\rho k_v k_g \sigma^g \mu_2(t) \\ & \frac{dT}{dt} = -\frac{UA}{MC_p}(T - T_j) \\ & 0 \le t \le t_f, \\ & T_{min} \le T \le T_{max}, \\ & T_{j\,min} \le T_j \le T_{j\,max}, \\ & \sigma_{min} \le \sigma \le \sigma_{max}, \\ & \left|\frac{dC_s}{dt}\right| \le k_1 \end{aligned} \tag{7}$$

$$n(0, t) \le n_{fine}, \forall \ t \ge t_f/2 \tag{8}$$

where $T_{min}$ and $T_{max}$ are the constraints on the crystallizer temperature, $T$, and are specified as 4°C and 22°C, respectively. $T_{j\,min}$ and $T_{j\,max}$ are the constraints on the manipulated variable, $T_j$, and are specified as 3°C and 22°C, respectively. The constraints on the supersaturation

$\sigma$ are $\sigma_{min} = 1.73$ and $\sigma_{max} = 2.89$. The constant, $k_1$, (chosen to be 0.065mg/ml·min) specifies the maximum rate of change of the saturation concentration $C_s$. $n_{fine}$ is the largest allowable number of nuclei at any time instant during the second half of the batch run, and is set to $5/\mu m.ml$. Previous work has shown that the objective of maximizing the volume-averaged crystal size can result in a large number of fines in the final product [12]. The constraint of Eq.8, by restricting the number of nuclei formed at any time instant during the second half of the batch run limits the fines in the final product. In the simulation, $\Delta t$ and $t_f$ are chosen as 5 minutes and 24 hours, respectively. The optimization problem is solved using sequential quadratic programming (SQP). A second-order accurate finite difference scheme with 3000 discretization points is used to obtain the solution of the population balance model of Eq.1.

## IV. Closed-loop simulation results

We considered first the case of no process-model mismatch, and then to investigate the effect of model inaccuracy on the ability of the predictive controller to control the crystallizer, we also consider a case of process–model mismatch by changing the value of the parameter $g$ (the exponent relating growth rate to supersaturation) from its nominal value of 5.169 to 4.652 (a 10% change) in the predictive controller. To study the ability of the proposed predictive control strategy to maximize the performance objective while avoiding the formation of a large number of fines in the final product, the predictive controller of Eq.7 is implemented with the additional constraint (Eq.8) on the fines in the final product. The simulation results under the predictive controller are compared with the simulation results obtained under the strategies of CTC and CSC and are shown in Figures 1–3 and Table II.

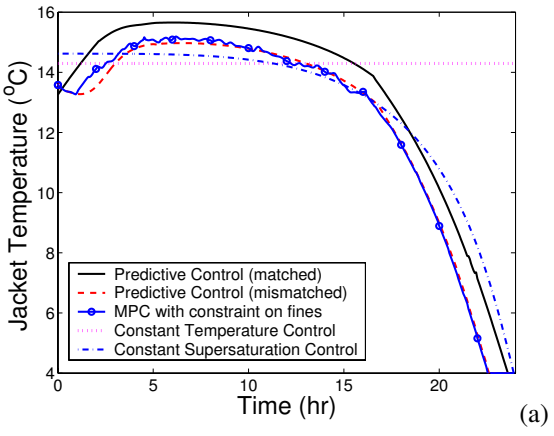


Fig. 1. Comparison of the simulation results for jacket temperature under five different control strategies.

In Figures 1-2, three important variables, the jacket temperature, the supersaturation, and the volume distribution of the CSD ($P(r)$) at the end of the batch run, are shown. The

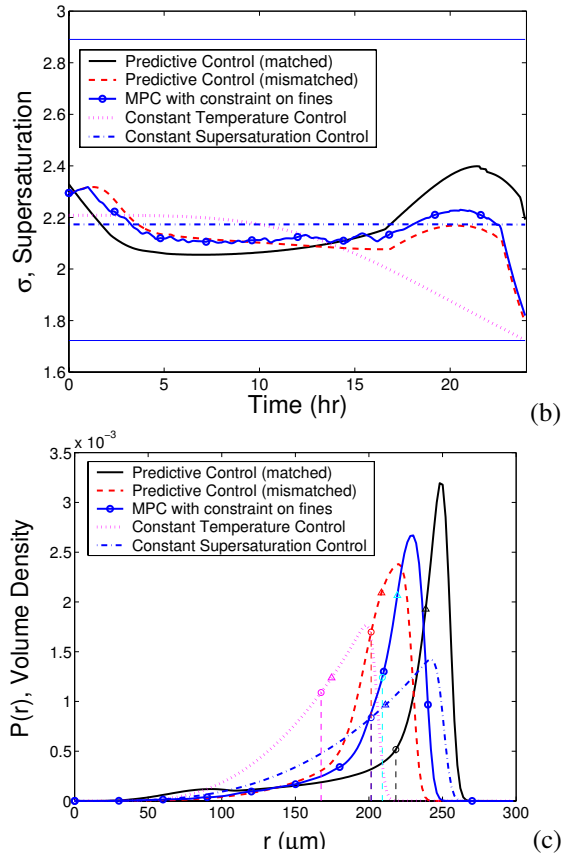


Fig. 2. Comparison of the simulation results for (a) supersaturation, and (b) volume density under five different control strategies.

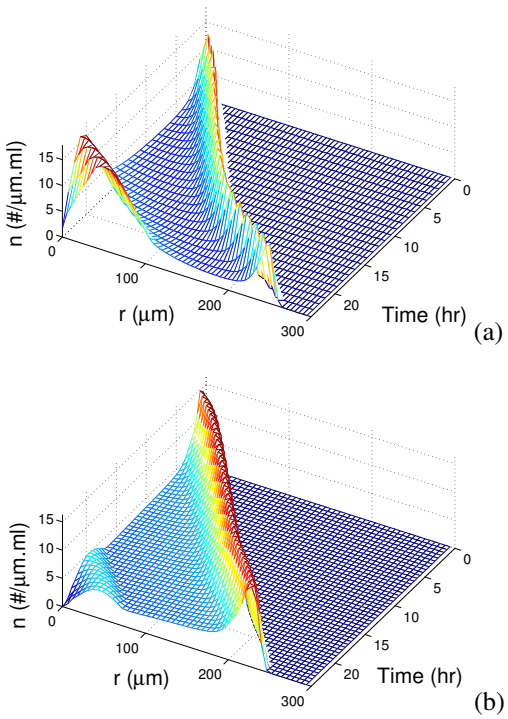


Fig. 3. Evolution of particle size distribution under (a) Predictive control with matched model, and (b) Predictive control with constraint on fines.

volume distribution of the CSD, $P(r)$, defined as:

$$P(r) = \frac{r^3 n(r, t_f)}{\int_0^\infty r^3 n(r, t_f) dr} \quad (9)$$

where $t_f$ is the time at the end of the batch run, is an important variable in determining the product characteristics. The two horizontal lines at 1.73 and 2.89 in Figure 2(a) are the lower and upper constraints on the supersaturation. The evolution of the CSD under the predictive control strategies is shown in Figure 3.

Figure 1 shows the comparison of the manipulated variable trajectories, the jacket temperature $T_j$, for the five scenarios. Note that while the trajectories of the jacket temperature under CSC (dash-dotted line) and under the predictive controller with a matched model (solid line) are close, the slight difference causes the behavior of CSD evolution under these two different control strategies to be significantly different, indicating the necessity to implement tight control to achieve a desired product quality.

Since the supersaturation $\sigma$ is the main driving force for crystal nucleation and growth, the evolution of the supersaturation under various control strategies, shown in Figure 2(a), can be used to explain the behavior of the CSD evolution. Specifically, the solid line in Figure 2(a) shows that the predictive controller computes a manipulated input trajectory that results in the supersaturation first decreasing, then staying almost constant at a low level, and finally increasing at the end of the batch run. In view of the fact that the control objective is to maximize the volume-averaged crystal size at the end of the batch run, i.e., to maximize the volume of big crystals while minimizing the volume of small crystals, the result can be understood as follows: after high initial levels of supersaturation, that results in a number of nuclei formed, a drop in the supersaturation results in the nucleation rate dropping more drastically than the growth rate (note that while the nucleation rate in Eq.2 shows exponential dependence on the supersaturation, the growth rate in Eq.2 exhibits a power law dependence), and favors growth of the initially formed crystals instead of formation of new crystals. Towards the end of the batch run, it is advantageous to increase the growth rate (by increasing the supersaturation) to maximize the size of the crystals in the batch reactor, even at the cost of forming a small number of new nuclei because the net result is a favorable increase in the volume-averaged crystal size.

Note that towards the end of the batch run, the solute concentration has depleted due to the formation of crystals. Supersaturation, however, is the solute concentration in excess of the solubility, and can be increased by decreasing the solubility, which is a function of the reactor temperature. Therefore, the desired increase in the supersaturation at the end of the batch run is achieved by lowering the jacket temperature (to lower the reactor temperature, which lowers the solubility, and hence, increases the supersaturation), until it hits the lower constraint (4 $^o$C) on the jacket temperature.

The closed-loop simulation results for the case of a process–model mismatch are shown by the dashed line in Figures 1 and 2. Comparing the solid lines and the dashed lines in Figure 2(a), it is clear that through feedback, the predictive controller 'corrects' for plant-model mismatch and produces a different manipulated input trajectory to enforce constraint satisfaction and achieve the desired objective. Simulation results, not included here for the sake of brevity, also demonstrate that if the off-line optimized trajectory of jacket temperature, based on the mismatched model, is implemented for the entire duration of the batch run without using the measurements to update the control trajectory, the state constraints are violated at the end of the batch run underscoring the importance of feedback to achieve robustness with respect to modeling errors.

Note that predictive control without constraint on fines can result in a product with a large number of fines (see Figure 3(a)) which is undesirable. The implementation of the predictive controller with the constraint of Eq.8, designed to reduce the fines in the product, results in a product with much less fines while still maximizing the volume-averaged crystal size (see Figure 3(b) and Table II).

Compared to predictive control, the crystal size distribution evolves very differently under CTC and CSC. Under CTC, where a constant reactor temperature is maintained throughout the batch run, the control strategy results in a constant solubility during the batch run, and the depletion in the concentration is reflected in the decrease of supersaturation, which eventually hits its lower constraint (the dotted line in Figure 2(a)). In contrast, under CSC, which tries to maintain a constant value of the supersaturation during the entire batch run, the reactor temperature is lowered during the entire batch run (via the continued lowering of the jacket temperature) to keep up with the falling concentration levels (see the dash-dotted line in Figures 1 and 2(a)). Under CSC, therefore, the growth rate stays constant during the batch run, since it is only dependent on the supersaturation. The nucleation rate, which also depends directly on the solute concentration itself, is lowered gradually because of the depletion of the solute. Unlike the CSD evolution under predictive control, in the case of CTC and CSC, a constant number of new nuclei are continuously formed during the whole batch run until the depletion of the solute and this leads to a relatively low volume-averaged crystal size compared to the case of crystallizer operation under predictive control.

Table II summarizes the simulation results obtained under the five different control strategies: (1) Predictive control with a matched model, (2) Predictive control with a mismatched model, (3) Predictive control with constraint on fines, (4) Open-loop operation under CTC, and (5) Open-loop operation under CSC. In Table II, six characteristic parameters of the product at the end of the batch run are compared, including the value of the volume-averaged crystal size ($\mu_4/\mu_3$), total volume ($\mu_3$), $r_{10}$, $r_{50}$, $r_{90}$ and the span. $r_{10}$, $r_{50}$ and $r_{90}$ are the 10%, 50% and 90% volume

fractions of the CSD, respectively, denoting the percentage of crystals smaller than that size. The span, defined as $(r_{90} - r_{10})/r_{50}$, is an important characteristic of the CSD, and is widely used in the pharmaceutical industry. A high span value indicates a wide distribution in size and a high polydispersity, which is undesirable.

Comparing the results of the five control strategies listed in Table II, it is clear that the predictive controller increases the volume-averaged crystal size by 30% compared to CTC, and 8.5% compared to CSC. It is also observed that, in the case of process–model mismatch (a 10% error of the exponent relating growth rate to supersaturation), the predictive control strategy is able to increase the volume-averaged crystal size by 20% compared to CTC. Although the predictive controller with a mismatched model results in a similar volume-averaged crystal size compared to CSC, it leads to a much higher volume of the product, 103% compared to CTC and 16% compared to CSC. Note also that the CSD under predictive control has the largest $r_{10}$, $r_{50}$ and $r_{90}$. Figure 2(b) shows that the CSDs under the proposed predictive controller with perfect model (solid line), plant-model mismatch (dashed line) and constraint on fines (solid line marked with circles) have lower polydispersity. A lower span and much larger volume-averaged crystal size are achieved under predictive control with constraint on fines compared to the one under CTC and CSC, as shown in Table II. In summary, the implementation of the proposed predictive controller increases the volume-averaged crystal size, satisfies state and input constraints, and is found to be robust with respect to plant-model mismatch.

TABLE II

COMPARISON BETWEEN THE SIMULATION RESULTS UNDER FIVE DIFFERENT CONTROL STRATEGIES.

| Control Strategy | $\mu_4/\mu_3$ | $\mu_3$ | $r_{10}$ | $r_{50}$ | $r_{90}$ | Span |
|---|---|---|---|---|---|---|
| | $\mu m$ | $\times 10^3$ | $\mu m$ | $\mu m$ | $\mu m$ | |
| Predictive control (matched) | 218 | 5.589 | 143 | 239 | 253 | 0.463 |
| Predictive control (mismatched) | 201 | 6.459 | 167 | 208 | 226 | 0.284 |
| Predictive control with constraint on fines | 208 | 6.374 | 166 | 219 | 235 | 0.315 |
| Open-loop CTC | 168 | 3.186 | 123 | 175 | 201 | 0.445 |
| Open-loop CSC | 201 | 5.583 | 143 | 211 | 244 | 0.478 |

## REFERENCES


[1] F. Rosenberger, S. B. Howard, J. W. Sowers, and T. A. Nyce, "Temperature dependence of protein solubility – determination and application to crystallization in x-ray capillaries," *Journal of Crystal Growth*, vol. 129, pp. 1–12, 1993.

[2] L. A. Monaco and F. Rosenberger, "Growth and etching kinetics of tetragonal lysozyme," *Journal of Crystal Growth*, vol. 129, pp. 465–484, 1993.

[3] F. Rosenberger and E. J. Meehan, "Control of nucleation and growth in protein crystal growth," *Journal of Crystal Growth*, vol. 90, pp. 74–78, 1988.

[4] C. A. Schall, J. S. Riley, E. Li, E. Arnold, and J. M. Wiencek, "Application of temperature control strategies to the growth of hen egg-white lysozyme crystals," *Journal of Crystal Growth*, vol. 165, pp. 299–307, 1996.

[5] S. K. Friedlander, *Smoke, Dust, and Haze: Fundamentals of Aerosol Behavior*. New York: Wiley, 1977.

[6] F. Gelbard and J. H. Seinfeld, "Numerical solution of the dynamic equation for particulate processes," *J. Comp. Phys.*, vol. 28, pp. 357–375, 1978.

[7] D. Ramkrishna, "The status of population balances," *Rev. Chem. Eng.*, vol. 3, pp. 49–95, 1985.

[8] S. Kumar and D. Ramkrishna, "On the solution of population balance equations by discretization-II. a moving pivot technique," *Chem. Eng. Sci.*, vol. 51, pp. 1333–1342, 1996.

[9] G. R. Jerauld, Y. Vasatis, and M. F. Doherty, "Simple conditions for the appearance of sustained oscillations in continuous crystallizers," *Chem. Eng. Sci.*, vol. 38, pp. 1675–1681, 1983.

[10] J. B. Rawlings and W. H. Ray, "Stability of continuous emulsion polymerization reactors: a detailed model analysis," *Chem. Eng. Sci.*, vol. 42, pp. 2767–2777, 1987.

[11] A. D. Randolph and M. A. Larson, *Theory of Particulate Processes*. San Diego: Academic press, Second edition, 1988.

[12] D. L. Ma, D. K. Tafti, and R. D. Braatz, "Optimal control and simulation of multidimensional crystallization processes," *Comp. & Chem. Eng.*, vol. 26, pp. 1103–1116, 2002.

[13] P. D. Christofides, *Model-Based Control of Particulate Processes*. Kluwer Academic Publishers, 2002.

[14] D. Semino and W. H. Ray, "Control of systems described by population balance equations-I. controllability analysis," *Chem. Eng. Sci.*, vol. 50, pp. 1805–1824, 1995.

[15] ——, "Control of systems described by population balance equations-II. emulsion polymerization with constrained control action," *Chem. Eng. Sci.*, vol. 50, pp. 1825–1839, 1995.

[16] S. Rohani and J. R. Bourne, "Self-tuning control of crystal size distribution in a cooling batch crystallizer," *Chem. Eng. Sci.*, vol. 12, pp. 3457–3466, 1990.

[17] J. Dimitratos, G. Elicabe, and C. Georgakis, "Control of emulsion polymerization reactors," *AIChE J.*, vol. 40, pp. 1993–2021, 1994.

[18] T. Chiu and P. D. Christofides, "Nonlinear control of particulate processes," *AIChE J.*, vol. 45, pp. 1279–1297, 1999.

[19] ——, "Robust control of particulate processes using uncertain population balances," *AIChE J.*, vol. 46, pp. 266–280, 2000.

[20] N. H. El-Farra, T. Chiu, and P. D. Christofides, "Analysis and control of particulate processes with input constraints," *AIChE J.*, vol. 47, pp. 1849–1865, 2001.

[21] S. M. Miller and J. B. Rawlings, "Model identification and control strategies for batch cooling crystallizers," *AIChE J.*, vol. 40, pp. 1312–1327, 1994.

[22] A. K. W. Leung, M. M. V. Park, and D. W. Borhani, "An improved method for protein crystal density measurements," *Journal of Applied Crystallography*, vol. 32, pp. 1006–1009, 1999.

[23] D. Shi, P. Mhaskar, N. H. El-Farra, and P. D. Christofides, "Predictive control of particle size distribution in protein crystallization," submitted*, Nanotechnology*, 2005.

[24] H. M. Hulburt and S. Katz, "Some problems in particle technology: A statistical mechanical formulation," *Chem. Eng. Sci.*, vol. 19, pp. 555–574, 1964.

[25] D. Shi, N. H. El-Farra, M. Li, P. Mhaskar, and P. D. Christofides, "Predictive control of particle size distribution in particulate processes," to appear*, Chem. Eng. Sci.*, 2005.

[26] J. B. Rawlings, S. M. Miller, and W. R. Witkowski, "Model identification and control of solution crystallizatin process – a review," *Ind. Eng. Chem. Res.*, vol. 32, pp. 1275–1296, 1993.

[27] W. Xie, S. Rohani, and A. Phoenix, "Dynamic modeling and operation of a seeded batch cooling crystallizer," *Chem. Eng. Comm.*, vol. 187, pp. 229–249, 2001.

[28] J. W. Mullin and J. Nyvlt, "Programmed cooling of batch crystallizers," *Chem. Eng. Sci.*, vol. 26, pp. 369–377, 1971.

[29] G. P. Zhang and S. Rohani, "On-line optimal control of a seeded batch cooling crystallizer," *Chem. Eng. Sci.*, vol. 58, pp. 1887–1896, 2003.